ADVANCED FUNCTIONAL MATERIALS
www.afm-journal.de

Inkjet Printing of MoS_2

*Jiantong Li, Maziar M. Naiini, Sam Vaziri, Max C. Lemme, and Mikael Östling**

A simple and efficient inkjet printing technology is developed for molybdenum disulfide (MoS_2), one of the most attractive two-dimensional layered materials. The technology effectively addresses critical issues associated with normal MoS_2 liquid dispersions (such as incompatible rheology, low concentration, and solvent toxicity), and hence can directly and reliably write uniform patterns of high-quality (5–7 nm thick) MoS_2 nanosheets at a resolution of tens of micrometers. The technology efficiency facilitates the integration of printed MoS_2 patterns with other components (such as electrodes), and hence allows fabricating various functional devices, including thin film transistors, photoluminescence patterns, and photodetectors, in a simple, massive and cost-effective manner while retains the unique properties of MoS_2. The technology has great potential in a variety of applications, such as photonics, optoelectronics, sensors, and energy storage.

1. Introduction

Because of their unique properties, two-dimensional (2D) layered materials have attracted great interest in various research fields.[1–4] Besides the most prominent graphene, molybdenum disulfide (MoS_2) is now widely regarded as a promising material for electronics and optoelectronics.[5–9] Superior transistors[5] (mobility >200 $cm^2\ V^{-1}\ s^{-1}$ and on/off current ratio ~10^8) and very sensitive photodetectors[6] have been demonstrated based on single-layer MoS_2 flakes. In addition, devices made from few-layer or multilayer MoS_2 flakes also exhibit excellent performance.[7–9] In spite of the high device performance, these MoS_2 flakes are mainly obtained from the low-yield mechanical cleavage technique. Recently, chemical vapor depositions have been developed to produce large-scale MoS_2.[10,11] However, as for the emerging macro-electronics[12,13] which features cost efficiency, simple methods to fabricate solution-phase MoS_2 nanosheets are favorable in a variety of applications, such as sensors,[14] photodetectors,[15,16] and supercapacitors.[17] Furthermore, patterning,[18] especially direct patterning,[17] of MoS_2 at micrometer dimensions has great significance in extending their applications. As a powerful direct writing technique,[19] inkjet printing has received increasing interest in electronics.[13,20] Great progress has recently been made in developing inkjet printing technology for graphene.[21,22] In this work, we have established a reliable and efficient inkjet printing technology for MoS_2.

Similar to graphene, massive MoS_2 nanosheets can be conveniently obtained from sonicating bulk MoS_2 powders in an appropriate organic solvent, such as dimethylformamide (DMF) and N-methyl-pyrrolidone (NMP).[1–3,23] With the pretreatments of bulk MoS_2 powders through grinding[14] or intercalation by alkali ions,[24,25] MoS_2 nanosheets can be effectively exfoliated in water. In general, however, none of the as-prepared MoS_2 dispersions are excellent for inkjet printing. They usually suffer from low viscosity (<2 cP, as compared with the value about 10 cP favored by inkjet printing), short stable period, low concentration and/or solvent toxicity. The incompatible viscosity may reduce the controllability of droplet jetting, while unstable inks may cause flake aggregation during the printing course and block the nozzles. Both of them severely degrade the reliability of inkjet printing especially when small scale (down to the level of 100 μm) is required. The low concentration diminishes the printing efficiency, and the solvent toxicity causes environmental concerns. As a matter of fact, in spite of experimental attempts in the field,[14,23,24] no efficient inkjet printing technology has been demonstrated for mass production of MoS_2 patterns/devices in sub-mm scale. In this work we combine the solvent exchange[21,26] and polymer stabilization[27] techniques developed for graphene dispersions to address the above issues concerning inkjet printing of MoS_2. First, bulk MoS_2 powders are exfoliated in DMF through bath sonication and high-speed centrifugation to obtain thin and small MoS_2 nanosheets. The nanosheets are then stabilized by a small amount of polymers, ethyl cellulose (EC). Finally, the solvent DMF is exchanged with terpineol through distillation at a high volume ratio (DMF:terpineol = 20:1), by virtue of the significant difference in boiling point between DMF (boiling point ~ 150°C) and terpineol (boiling point ~220 °C). Consequently, the solvent is exchanged from the low-viscosity (0.9 cP at 20 °C) and toxic DMF to high-viscosity (~40 cP at 20 °C) and nontoxic terpineol, and meanwhile the MoS_2 concentration is significantly increased. Mixing with ethanol, the rheology of MoS_2/terpineol dispersions may be tailored to be compatible with inkjet printing. As a result, all the critical challenges have been overcome, and efficient and reliable inkjet printing can be

Dr. J. Li, M. M. Naiini, S. Vaziri, Prof. M. C. Lemme, Prof. M. Östling
KTH Royal Institute of Technology
School of Information and Communication Technology
Electrum 229, SE-164 40 Kista, Sweden
E-mail: ostling@kth.se
Prof. M. C. Lemme
University of Siegen
Hölderlinstr. 3, 57076 Siegen, Germany

DOI: 10.1002/adfm.201400984

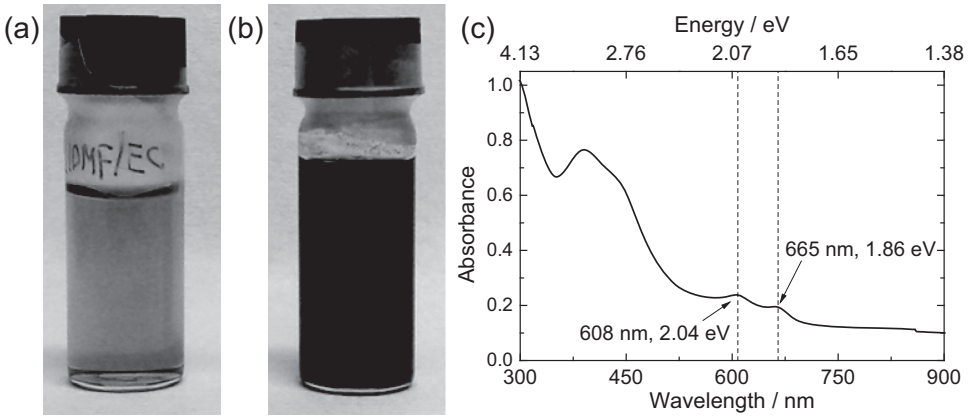

Figure 1. MoS_2 inks. a) Photograph of the MoS_2/DMF dispersion before distillation. The MoS_2 nanosheets have been stabilized by EC. b) Photograph of the final MoS_2/terpineol ink. As compared with the initial MoS_2/DMF dispersion in (a), the MoS_2/terpineol ink is first concentrated by 20 times via distillation and then tailored by ethanol at the volume ratio of terpineol:ethanol = 3:1. c) Absorbance spectra for the MoS_2 ink in (b) diluted by 20 times with terpineol.

attained at the resolution of tens of micrometers (the limit of a normal inkjet printer).

2. Result and Discussion

Figure 1 shows the dilute MoS_2/DMF dispersion stabilized by EC (Figure 1a) and the final MoS_2/terpineol ink tailored with ethanol (Figure 1b). The color change of the dispersion from dark yellow (Figure 1a) to black (Figure 1b) suggests a significant increase in the MoS_2 concentration. Figure 1c indicates the absorbance spectra for the final MoS_2 ink diluted by 20 times with terpineol. The two characteristic peaks around 600 nm and 672 nm confirm the existence of MoS_2.[2,14,25] Using the Lambert-Beer law and the extinction coefficient at 672 nm α_{672} = 3400 mL/(mg·m),[2] we estimate the MoS_2 concentration in our final ink to be ~ 0.1 mg/mL. The ink is stable (without occurrence of any visible sediments) for one week when staying still. During printing, the ink in the cartridge keeps on moving, which suppresses the flake aggregation and extends the ink stability (without evidently clogging the nozzles) to 2~3 weeks. We also prepared MoS_2 inks with higher concentration through increasing the volume ratio of DMF: terpineol to 60:1, but the resulting ink was only stable for about 4 h (staying still). The attained concentration of 0.1 mg/mL and simultaneous stable period of one week have already approached the best quality of MoS_2 dispersions.[2] We regard EC as an excellent stabilizer for MoS_2 inks because it can also improve the uniformity of printed patterns,[21,22,27] prevent flake restacking,[28] and importantly, be readily removed through a simple annealing[21,22,27] so that the residual contamination is insignificant.

Using an inkjet printer (Dimatix DMP 2800), we have demonstrated excellent jetting performance for the MoS_2 inks. As shown in Figure S1, the MoS_2 ink droplets are well directed and constantly jetted out of all nozzles at an even velocity. The reliable jetting performance enables us to print various patterns at large scale. **Figure 2** shows the printed drop matrix, lines and film on untreated Si/SiO_2 substrates with a resolution (droplet diameter or line width) of ~80 μm. The as-printed patterns (Figure 2a–c) conform well to the designs, and after drying, they exhibit good uniformity (Figure 2d–f). Somewhat, however, the MoS_2 patterns suffer from the undesired coffee-ring effects (perimeter is thicker than interior, as clearly seen in Figure 2f). The coffee-ring effects, caused by the pinning of contact lines,[29] are general phenomena during the drying of liquid drops. The contact line pinning is also observed for our MoS_2 inks (Movie V1 in Supporting Information). In contrast, with similar ink composition, the graphene inks can unpin the contact lines so that the coffee-ring effects are suppressed.[21] This clear difference between graphene and MoS_2 inks is interesting and deserves further extensive studies.

The technology allows convenient and massive production of electronic devices based on MoS_2 nanosheets. **Figure 3**a shows the inkjet printed MoS_2 devices with printed silver electrodes on a SiO_2/Si substrate (the SiO_2 layer is 300 nm thick). The devices have been annealed at 450 °C in N_2 atmosphere to remove the stabilizing polymer. During annealing, the N_2 atmosphere is needed to protect MoS_2 from being oxidized. The Raman spectra of the printed MoS_2 films (Figure 3b) exhibit two characteristic peaks at 383.0 and 408.2 cm^{-1}, corresponding to the E^1_{2g} and A_{1g} modes, respectively. The frequency distance between the two peaks is 25.2 cm^{-1}, suggesting that most MoS_2 flakes have more than 6 layers (a systematic study[30] suggests the peak distance increases with the MoS_2 layer numbers and 6-layer MoS_2 flake has a peak distance ~24.8 cm^{-1}). The morphology of the printed MoS_2 films are characterized through atomic force microscopy (AFM) and scanning electron microscopy (SEM). Both AFM (Figure 3c) and SEM (Figure 3d) images indicate that after annealing, the microstructure of the MoS_2 films appears in the form of percolation clusters, rather than uniformly distributed flakes. This is consistent with other observation of pinholes in films of centrifuged MoS_2 nanosheets.[16] It is likely that phase separation[31] (between MoS_2 and EC) takes place during annealing and hence form the percolation-cluster-like microstructure. The zoom-in view of the AFM images on the void region (Figure S2) shows many isolated individual MoS_2 flakes. From the cross-section profile analysis (Figure S2), we find most MoS_2 flakes to be about 5–7 nm thick with the lateral dimension ranging from 40 nm to 100 nm (there are a small amount of MoS_2 flakes larger than

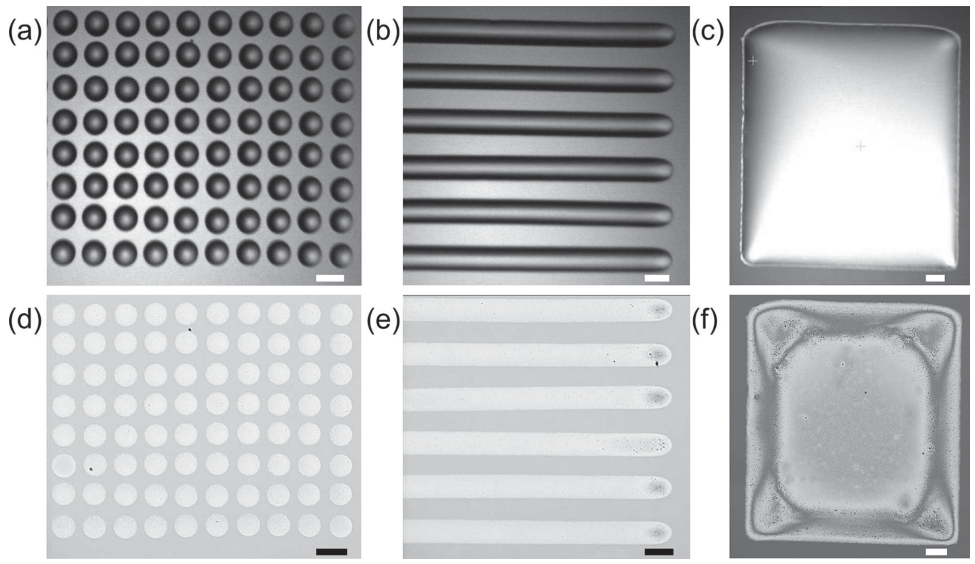

Figure 2. Optical micrographs of inkjet printed MoS_2 patterns. a) As-printed droplet matrix. b) As-printed lines. c) As-printed film. d,e,f) are dried patterns of (a), (b) and (c), respectively. All scale bars are 100 μm.

100 nm, Figure S3). The flake thickness is consistent with the Raman spectra in Figure 3b (note 6 MoS_2 layers correspond to a thickness of ~4.2 nm). The zoom-in view of the SEM images on the percolation clusters (Figure 3e) indicates randomly distributed MoS_2 flakes (note during annealing, the N_2 atmosphere retards the decomposition of EC so that some polymer residue is still visible in Figure 3e). The annealed MoS_2 films actually constitute a double-level hierarchical percolation system:[31,32] The first level is the apparent percolation clusters (Figure 3c,d) while each cluster comprises random MoS_2 flakes (Figure 3e) which form the second-level percolation. Double-level percolation systems usually possess significantly lower percolation

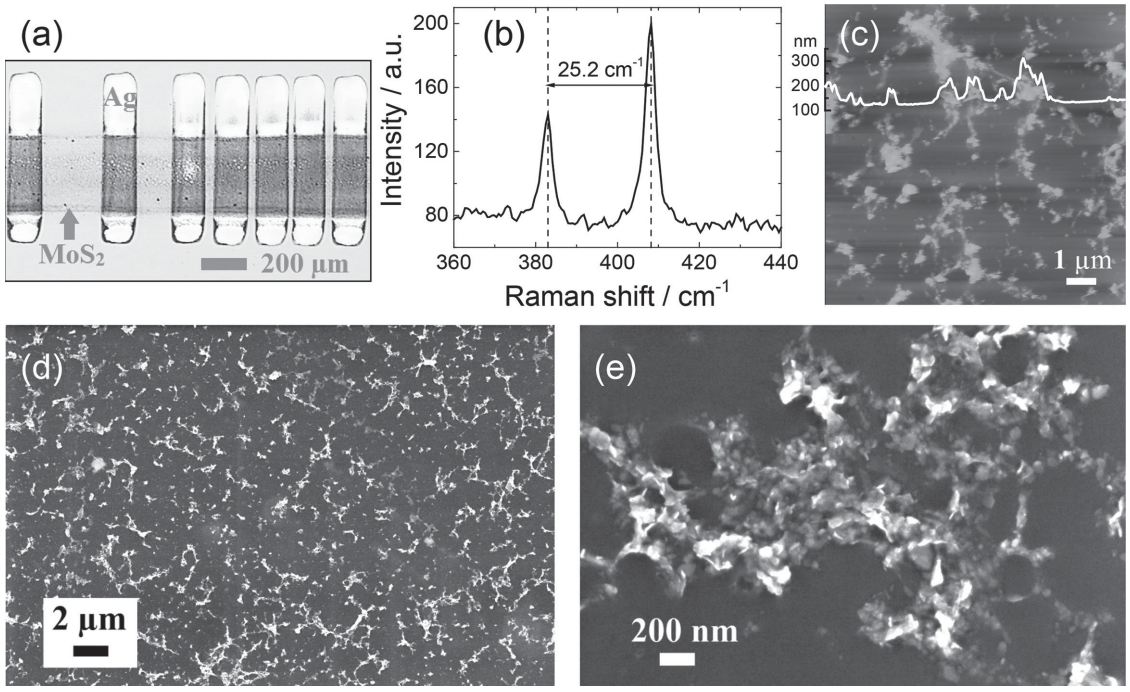

Figure 3. Inkjet printed MoS_2 devices on SiO_2/Si substrates (the SiO_2 layer is 300 nm thick). a) Optical micrograph of the printed devices. The vertical strips are inkjet printed silver electrodes, and the horizontal line (~350 μm wide) is the printed MoS_2 channel (at the drop spacing of 20 μm and with 3 printing passes). For electrical passivation, the whole devices have been covered by a layer of 50-nm-thick Al_2O_3 via atomic layer deposition which makes the substrates appear yellow. All morphology studies were performed without the Al_2O_3 deposition. b) Raman spectra, c) AFM image, d) SEM image, and e) zoom-in SEM image on the MoS_2 (channel) region in (a).

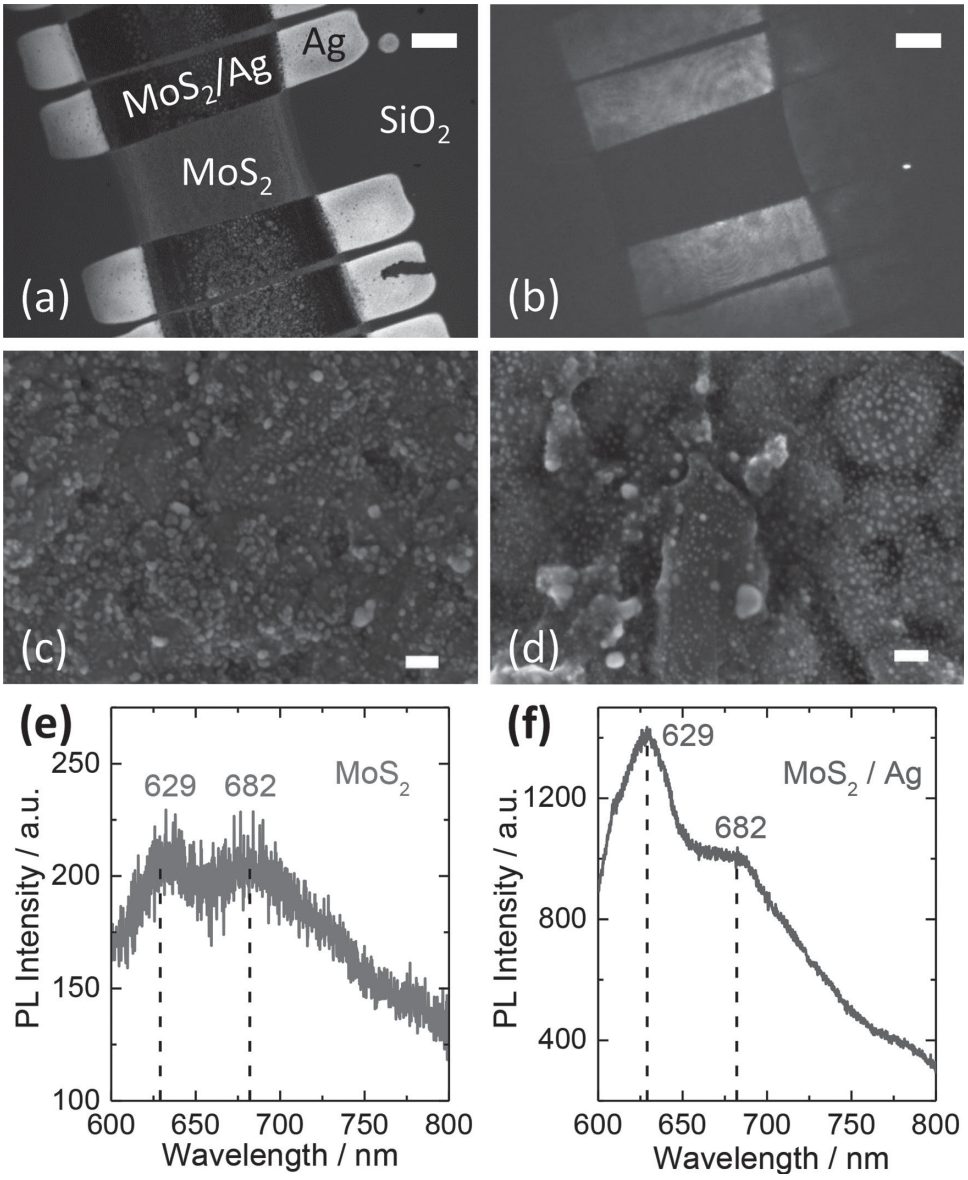

Figure 4. Photoluminescence of printed MoS_2 on SiO_2/Si substrates. a) Optical micrograph of the printed devices under illumination of white light. b) PL image of the devices in (a) under illumination of an excitation laser (wavelength 532 nm). c,d) SEM images of c) silver electrodes and d) MoS_2 on top of silver electrodes. e,f) PL spectra of e) MoS_2 on SiO_2/Si substrates and f) MoS_2 on top of silver electrodes. The PL image (b) and spectra (e,f) were measured after an optical filter (longpass > 560 nm). Scale bars are 100 μm in (a) and (b), and 100 nm in (c) and (d).

thresholds (approximate to the products of the percolation thresholds for the two levels).[31,32] In our case, most MoS_2 flakes are locally concentrated to the percolation clusters so that the global spanning probability is evidently higher than that of a uniform film with the same amount of MoS_2. Consequently, much less MoS_2 flakes are required to percolate the systems, which is a desired merit for conductance improvement. To confirm the percolation effects, we study the dependence of the MoS_2 film conductivity σ on the number of printing passes N, as shown in Figure S4 where the drop spacing is 40 μm in the printing process. When $N \geq 15$, σ is almost independent of N which is expected for bulk-like materials. However, at small N region ($N < 15$), σ significantly increases with N as a power law $\sigma \sim (N\text{-}N_0)^n$ with $N_0 \approx 3.6$ and $n \approx 1.7$, suggesting the dominance of the percolation effects.[23]

Photoluminescence (PL) is observed from our printed MoS_2 devices (**Figure 4**). Figure 4a indicates some printed MoS_2 devices under illumination of white light, while Figure 4b shows their PL image under an excitation laser with wavelength 532 nm. Usually only single-layer MoS_2 can generate strong PL thanks to the direct bandgap, and PL severely decreases with increasing MoS_2 layer numbers.[10,25,33] Indeed, Figure 4b shows very weak PL from our printed MoS_2 (mostly > 6 layers) on the SiO_2/Si substrate. In contrast, however, the same MoS_2 on top of the silver electrodes generates very strong PL (the bright regions in Figure 4b). Note that this PL is also much stronger

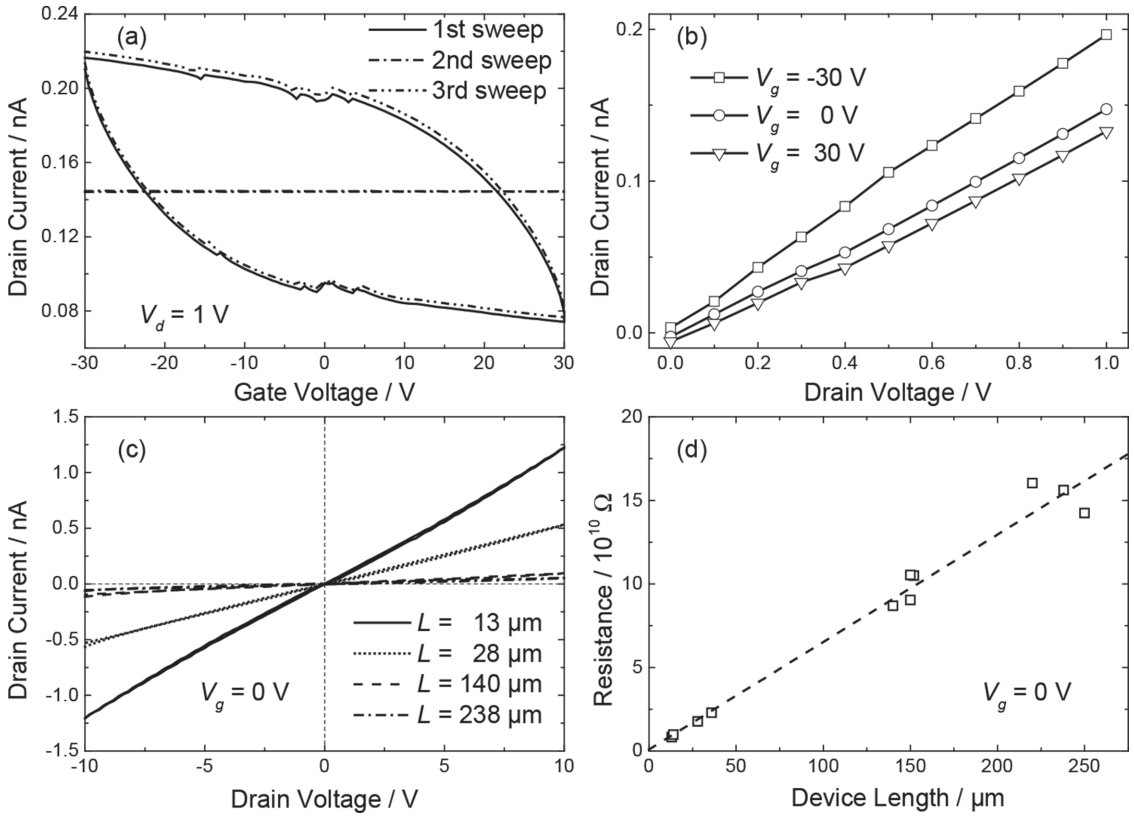

Figure 5. Electrical characterization of the printed MoS_2 TFTs. a) Transfer characteristics for a printed MoS_2 TFT (L = 13 μm). For each measurement, the gate voltage sweep is from −30 V to 30 V to −30 V. For the second sweep, the cable to the gate contact is physically disconnected. The invariant drain currents confirm the gate modulation in other sweeps. b) Output characteristics (drain current-drain voltage curves) at different gate bias for the device in (a). c) Drain current-drain voltage curves at V_g = 0 V for devices with different channel lengths. For each measurement, the drain voltage sweep is from −10 V to 10 V to −10 V. d) Dependence of device resistance (V_g = 0 V) on the channel length. The symbols are experimental data and the line is the linear fitting.

than that from the pure silver electrode. As shown in Figure 4c, the inkjet printed silver electrodes consist of many silver nanoparticles (mostly > 20 nm). Although these silver nanoparticles do not generate strong PL themselves, when attaching to the MoS_2 flakes (Figure 4d), they significantly enhance the PL from MoS_2.[34] Figures 4e and 4f display the PL spectra at the MoS_2 region and the MoS_2/silver region, respectively. The two characteristic peaks around 630 nm and 680 nm confirm that the PL should be ascribed to MoS_2.[10,25,33]

Furthermore, the silicon substrate is used as the back gate contact such that all devices are characterized as thin film transistors (TFTs), as shown in **Figure 5**. The transfer (Figure 5a) and output (Figure 5b) characteristics exhibit p-type gate modulation with a typical on/off current ratio around 2. The large hysteresis in Figure 5a implies the presence of charge traps on the MoS_2 flakes.[35,36] Although MoS_2 is intrinsically n-type semiconductor, liquid phase processing often introduces unintentional dopants or traps which may impact the electronic properties of MoS_2. As a result, low on/off current ratio (3 ~ 6) as well as p-type gate modulation are often observed in the literature for transistors based on liquid-exfoliated individual MoS_2 flakes.[2,37,38] However, previously demonstrated back-gate TFTs based on films of exfoliated MoS_2 nanosheets only exhibit negligible on/off current ratio (<1.1).[39] Our printed TFTs have comparable on/off current ratio to those based on individual liquid-exfoliated MoS_2 flakes, proving the efficiency of the printing technology. The current–voltage characteristics (Figure 5c) exhibit Ohmic behavior for all studied devices, while the resistance-length dependence (Figure 5d) indicates that the device resistance is almost proportional to the device length with a linear resistivity of 6.4×10^8 Ω/μm. Hence the silver-MoS_2 contact resistance is negligible. The linear resistivity corresponds to a conductivity of 8.9×10^{-5} S/m (the device width is ~350 μm and from the AFM image in Figure 3c we estimate the *average* film thickness to be no more than 50 nm). This value is even superior to that of the vacuum-filtered MoS_2 films (3.6×10^{-5} S/m).[2]

The printed MoS_2 devices exhibit very rapid photoresponse. **Figure 6** shows the time-resolved photoresponse for a device with channel length L = 13 μm. The device was biased at gate voltage V_g and drain voltage V_d, and illuminated by a Halogen lamp (OSRAM HLX 64653) through a microscope objective lens, as schematically illustrated in Figure 6a. The power density of the illuminating light beam (white light) was 0.35 mW/mm^2 (Figure S5). During the measurements, the light was alternately switched on/off at an interval of 5 s. Following each on/off switch, the device current (at V_g = 0 V and V_d = 1 V) swiftly jumps upwards/downwards and then returns toward the dark current

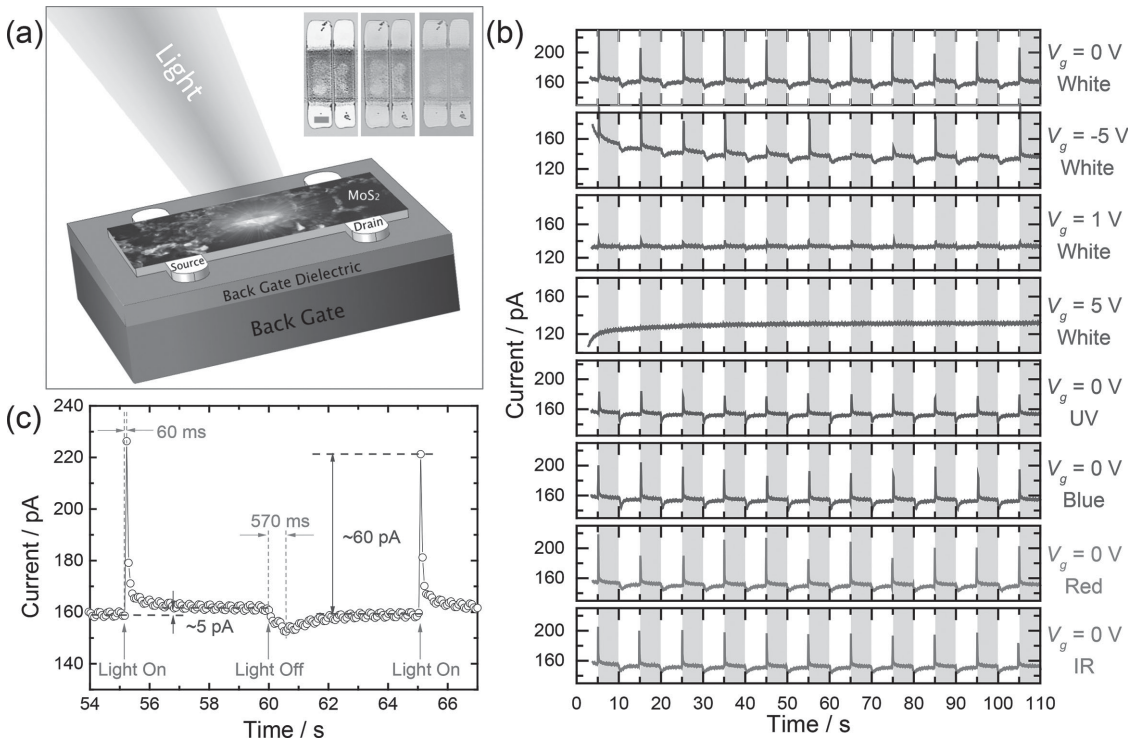

Figure 6. Photoresponse of a printed MoS_2 device (L = 13 μm). a) Illustration of the MoS_2 device structure under illumination. Upper-right inset: Optical micrographs of the device under different illuminations of white (left), blue (middle) and red (right) lights. The scale bar is 100 μm. b) Time-resolved photoresponse of the device under different gate bias V_g and/or different illuminations. The illuminations are produced by tuning the white light with appropriate THOR-labs colored glass filters (see Figure S9 for details). The lights are on (off) in the shaded (unshaded) intervals. Each interval is 5 s. c) A close-up view of the photoresponse to white light at V_g = 0 V [the topmost one in (b)]. In all measurements, V_d = 1 V.

level, resulting in a series of peaks and valleys. Surprisingly, the valleys may even fall below the dark currents (Figure 6b,c). The photoresponse significantly depends on the gate bias. For negative gate bias (V_g = -5 V in Figure 6b), the photoresponse retains but the peaks do not appear for every switch on. For positive gate bias, the photoresponse attenuates; the signal becomes very weak at $V_g = V_d$ and vanishes when $V_g > V_d$. Such behavior has been confirmed with two other devices (Figure S6). Therefore, the optimal operating condition is around V_g = 0 V. Actually, excellent photoresponse can be achieved even without the gate bias, i.e., under floating gate (Figure S7). This feature simplifies the device fabrication and operation. However, one should note that the optimal operating condition may vary with different substrates. For example, floating gate seems not to be the optimal operating condition for the printed MoS_2 devices on glass (Figure S8). Under floating gate, these devices (on glass) exhibit very similar photoresponse to those on SiO_2/Si wafers under positive V_g. With the assistance of appropriate glass filters (THOR-labs, FGK01 Kit, Figure S9), the illumination can be tuned from white light to ultraviolet (UV), blue, red and infrared (IR) lights (the inset in Figure 6a shows the device illuminated by different visible lights). Under all tested illumination conditions (V_g = 0 V), the peak/valley retains in response to every switch on/off, even in the case of the lowest-power UV light. From the close-up view of the current-time curves in Figure 6c, the rise time for the peak and fall time for the valley are around 60 ms and 570 ms, respectively. The response time is comparable to that of the photodetectors based on monolayer MoS_2.[6,40] In fact, the measured rise time (60 ms) is limited by the time resolution of our equipment and the true response time may be much shorter. Taking the average peak height (57 ± 11 pA for the white light at V_g = 0 V in Figure 6b) as the photocurrents, we estimate the photoresponsivity to be 36 ± 7 μA/W (the device area is 4.6×10^{-3} mm^2 and the received power is about 1.6 μW). Although this photoresponsivity is much lower than that of photodetectors based on individual MoS_2 flakes,[6,9,40] it is comparable to those based on individual carbon nanotubes[41] or graphene.[42–44] In particular, it is also comparable to that of MoS_2 nanosheet films fabricated by the Langmuir-Blodggett (LB) method,[16] implying that our inkjet printing processes do not induce obvious performance degradation.

The responsive peaks/valleys are highly reproducible (at V_g = 0 V or under floating gate) in all the printed photodetectors (Figures S6,S7). We have confirmed that these peaks/valleys are not caused by the light source (Figures S5,S10) or other electrical interferences (Figure S11), and should represent intrinsic response to the light switching. As shown in Figure 5c, a peak (valley) can be regarded as the combination of a fast rise (decay) and a sequent slow decay (rise) of the photocurrents. Similar behaviors are observed in other photodetectors based on MoS_2 nanosheets,[16] although there, a fast rise (decay) is followed by a slow rise (decay) of photocurrents. Similarly, we associate the current peaks and valleys with the presence of traps.[16] As soon as the light is switched on, the fast current rise is ascribed to the initial equilibration of carrier generation and recombination.[16]

Afterwards, carriers are trapped and the current slowly decays. This forms the upward peaks. Upon switching off the light, the generation rate drops abruptly so that the predominant carrier recombination gives rise to a fast current fall. The current may even transiently fall below the initial dark current level. Gradually, the thermal release of the trapped carriers leads to a slow current increase. This forms the downward valleys. The traps may also serve as the generation-recombination centers which assist the generation/recombination process so that long-wavelength illumination (such as IR) can also be detected. At negative V_g (on state), there are more carriers and the trapping is faster. The photo-generated carriers may be trapped immediately, which prevents the appearance of some peaks upon illumination. At positive V_g (off state), the photo-generation rate may decrease with increasing V_g (likely because of the enhanced detrapping process) and hence the photoresponse attenuates or even vanishes. Therefore, all response behavior should result from the coupling between photo-generation/recombination and trapping/detrapping processes. These characteristics are in essence consistent with those of MoS_2 photodetectors fabricated by the LB method.[16]

Finally, we would mention that although our MoS_2 inks are only stable for one week when staying still, the precipitated MoS_2 ink can be recovered by a rough sonication for one hour. Comparable jetting (Figure S12) and electrical (Figure S13) performance to those of the fresh inks can be obtained for the recovered MoS_2 ink which has even been stored for more than one year.

3. Conclusions

In conclusion, by employing the solvent exchange and polymer stabilization techniques, we have developed a reliable and efficient technology for inkjet printing of multilayer (>6 layers, 5–7 nm thick) MoS_2 nanosheets. Conformal and uniform patterns can be printed with a resolution of about 80 μm (limited by the standard low-resolution printer and without any optimization for the substrate surface). Integrating the printed MoS_2 nanosheets with printed silver nanoparticles, we have demonstrated a simple method to significantly enhance the photoluminescence of multilayer MoS_2. The fully printed MoS_2-based thin film transistors and photodetectors exhibit commendable performance verifying the retainability of MoS_2's unique properties after printing. Consequently, the inkjet printing technology allows efficient, massive and cheap production of functional devices without inducing evident degradation of the MoS_2 materials. Further performance boost is anticipated once the general issues have been addressed concerning unintentional dopants/impurities in liquid-exfoliated MoS_2. We expect the technology will play an important role in a variety of applications, including photonics, optoelectronics, sensors and energy storage.

4. Experimental Section

MoS_2 Exfoliation: First, a mixture of MoS_2 powder (~2 mg/mL, Sigma-Aldrich, product no. 69860) in DMF was sonicated (Branson 2510E-MTH bath ultrasonicator) for ~48 h. The resultant suspension was centrifuged at 10,000 rpm for 30 min to sediment thick flakes and the supernatant was harvested. The supernatant was centrifuged once more at 10,000 rpm for 30 min to ensure the removal of big flakes. Then, ethyl cellulose (0.25 mg/mL, viscosity 4 cP for 5%w/v in 80:20 toluene:ethanol, Sigma-Aldrich, product no. 200646) was added to the harvested supernatant and the dispersion was sonicated for ~1 h. Finally, another ethyl cellulose (0.25 mg/mL, viscosity 22 cP for 5%w/v in 80:20 toluene:ethanol, Sigma-Aldrich, product no. 200697) was added to obtain a stable MoS_2/DMF dispersion.

Solvent Exchange: Terpineol (5 mL, Sigma-Aldrich, product no. 86480) was added to MoS_2/DMF dispersion (100 mL). DMF was exchanged by terpineol through a vacuum distillation process using a Rotary Evaporator (Rotavapor R-205, BÜCHI Labortechnik AG). DMF began to evaporate when the dispersion was heated to 80 °C and the pressure was reduced to ~30 mbar. After DMF was boiled off, the remaining MoS_2/terpineol dispersion was harvested. Compared with the original DMF dispersion, MoS_2 in the final terpineol dispersion was concentrated by ~20 times. Prior to printing, the MoS_2/terpineol dispersion was mixed with ethanol at the volume ratio of 3:1 to tailor the viscosity and surface tension for inkjet printing.

Concentration Estimation: In order to estimate the final MoS_2 concentration, the final ink (50 μL) was diluted with terpineol (950 μL) and the optical absorbance A was measured by a Varian Cary 100 Bio UV–Vis Spectrophotometer, as presented in Figure 1c. Note around the characteristic peak position (λ = 672 nm), $A \approx 0.18$. Through the Lambert-Beer law $A/l = \alpha_{672}C$ (l = 1 cm is the cell length) and the absorption coefficient $\alpha_{672} = 3400$ mL/(mg·m),[2] the MoS_2 concentration C in the diluted ink is estimated to be ~5.3 μg/mL. Therefore, the MoS_2 concentration in the final ink (20 times higher) should be ~0.1 mg/mL. Note as declared in Supporting Information of Ref. [2], the extinction coefficient α_{672} may vary with solvents. Then the value of 0.1 mg/mL should only be regarded as a rough estimation of the MoS_2 concentration in the final inks.

Device Fabrication: The patterns and devices were fabricated using a commercial piezoelectric Dimatix Material Printer (DMP 2800, Dimatix-Fujifilm Inc.) equipped with a 10 pL cartridge (DMC-11610). Our formulated MoS_2 inks and the commercial silver inks (Cabot Conductive Ink CCI-300, Cabot Corporation) were used. The lines and film in Figure 2 were printed with the drop spacing of 40 μm and 30 μm, respectively. The devices in Figures 3–6 were printed on silicon wafers capped with a thermally grown SiO_2 layer (300 nm thick). Before printing, the wafers were cleaned with isopropanol. First, silver inks were printed (drop spacing of 20 μm, one printing layer, substrate at room temperature) as the electrodes and baked at 150 °C for 30 min. Then, MoS_2 inks were printed (drop spacing of 20 μm, 3 printing layers, substrate at 40 °C) as the channels. Finally, the devices were annealed at N_2 (100 sccm) atmosphere: The temperature ramped at 10 °C/min to 160 °C, retained at 160 °C for 20 min, then ramped at 10 °C/min to 450 °C and eventually retained at 450 °C for 1 h. Before electrical characterization, the annealed devices were covered by a 50-nm-thick Al_2O_3 layer through atomic layer deposition at 200 °C for passivation.

Electrical Characterization: All electrical properties were characterized using Keithley SCS4200 parameter analyzer with a probe station. For photoresponse measurement, the devices are illuminated by a Halogen lamp (OSRAM HLX 64653) through the microscope objective lens. The UV, blue, red, and IR lights were produced through filtering the white light with the THOR-labs colored glass filters (see Figure S9 for details). The switch of the illuminations was operated manually.

Supporting Information

Supporting Information is available from the Wiley Online Library or from the author.

Acknowledgements

The authors thank Ingemar Petermann (Swedish ICT Acreo), Ilya Sytjugov, Fatemeh Sangghaleh, and Miao Zhang for kind helps in device measurement and characterization. Support and sponsorship by the European Research Council through the Advanced Investigator Grant OSIRIS (No. 228229) and the Proof of Concept Grant iPUBLIC (No. 641416), the Swedish Research Council through the grant iGRAPHENE, and the Göran Gustafsson Foundation through the Young Researcher Prize (No. 1415 B) are gratefully acknowledged. M. C. Lemme acknowledges support from the European Research Council through the Starting Grant InteGraDe (No. 307311) and the German Research Foundation (LE 2440/1-1).

Received: March 27, 2014
Revised: June 5, 2014
Published online: August 22, 2014

[1] Q. H. Wang, K. Kalantar-Zadeh, A. Kis, J. N. Coleman, M. S. Strano, *Nat. Nanotechnol.* **2012**, *7*, 699.
[2] J. N. Coleman, M. Lotya, A. O'Neill, S. D. Bergin, P. J. King, U. Khan, K. Young, A. Gaucher, S. De, R. J. Smith, I. V. Shvets, S. K. Arora, G. Stanton, H.-Y. Kim, K. Lee, G. T. Kim, G. S. Duesberg, T. Hallam, J. J. Boland, J. J. Wang, J. F. Donegan, J. C. Grunlan, G. Moriarty, A. Shmeliov, R. J. Nicholls, J. M. Perkins, E. M. Grieveson, K. Theuwissen, D. W. McComb, P. D. Nellist, V. Nicolosi, *Science* **2011**, *331*, 568.
[3] V. Nicolosi, M. Chhowalla, M. G. Kanatzidis, M. S. Strano, J. N. Coleman, *Science* **2013**, *340*, 1226419.
[4] J. Li, M. Östling, *Phys. Rev. E* **2013**, *88*, 012101.
[5] B. Radisavljevic, A. Radenovic, J. Brivio, V. Giacometti, A. Kis, *Nat. Nanotechnol.* **2011**, *6*, 147.
[6] O. Lopez-Sanchez, D. Lembke, M. Kayci, A. Radenovic, A. Kis, *Nat. Nanotechnol.* **2013**, *8*, 497.
[7] S. Kim, A. Konar, W.-S. Hwang, J. H. Lee, J. Lee, J. Yang, C. Jung, H. Kim, J.-B. Yoo, J.-Y. Choi, Y. W. Jin, S. Y. Lee, D. Jena, W. Choi, K. Kim, *Nat. Commun.* **2012**, *3*, 1011.
[8] H. S. Lee, S.-W. Min, Y.-G. Chang, M. K. Park, T. Nam, H. Kim, J. H. Kim, S. Ryu, S. Im, *Nano Lett.* **2012**, *12*, 3695.
[9] D.-S. Tsai, K.-K. Liu, D.-H. Lien, M.-L. Tsai, C.-F. Kang, C.-A. Lin, L.-J. Li, J.-H. He, *ACS Nano* **2013**, *7*, 3905.
[10] Y.-H. Lee, X.-Q. Zhang, W. Zhang, M.-T. Chang, C.-T. Lin, K.-D. Chang, Y.-C. Yu, J. T.-W. Wang, C.-S. Chang, L.-J. Li, T.-W. Lin, *Adv. Mater.* **2012**, *24*, 2320.
[11] Y. Zhan, Z. Liu, S. Najmaei, P. M. Ajayan, J. Lou, *Small* **2012**, *8*, 966.
[12] D. Voss, *Nature* **2000**, *407*, 442.
[13] R. F. Service, *Science* **1997**, *278*, 383.
[14] Y. Yao, L. Tolentino, Z. Yang, X. Song, W. Zhang, Y. Chen, C. Wong, *Adv. Funct. Mater.* **2013**, *23*, 3577.
[15] K.-G. Zhou, N.-N. Mao, H.-X. Wang, Y. Peng, H.-L. Zhang, *Angew. Chem. Int. Ed.* **2011**, *50*, 10839.
[16] G. Cunningham, U. Khan, C. Backes, D. Hanlon, D. McCloskey, J. F. Donegan, J. N. Coleman, *J. Mater. Chem. C* **2013**, *1*, 6899.
[17] L. Cao, S. Yang, W. Gao, Z. Liu, Y. Gong, L. Ma, G. Shi, S. Lei, Y. Zhang, S. Zhang, R. Vajtai, P. M. Ajayan, *Small* **2013**, *9*, 2905.
[18] C. L. Stender, E. C. Greyson, Y. Babayan, T. W. Odom, *Adv. Mater.* **2005**, *17*, 2837.
[19] D. B. Chrisey, *Science* **2000**, *289*, 879.
[20] J. Li, T. Unander, A. L. Cabezas, B. Shao, Z. Liu, Y. Feng, E. B. Forsberg, Z.-B. Zhang, I. Jõgi, X. Gao, M. Boman, L.-R. Zheng, M. Östling, H.-E. Nilsson, S.-L. Zhang, *J. Appl. Phys.* **2011**, *109*, 084915.
[21] J. Li, F. Ye, S. Vaziri, M. Muhammed, M. C. Lemme, M. Östling, *Adv. Mater.* **2013**, *25*, 3985.
[22] E. B. Secor, P. L. Prabhumirashi, K. Puntambekar, M. L. Geier, M. C. Hersam, *J. Phys. Chem. Lett.* **2013**, *4*, 1347.
[23] D. J. Finn, M. Lotya, G. Cunningham, R. J. Smith, D. McCloskey, J. F. Donegan, J. N. Coleman, *J. Mater. Chem. C* **2014**, *2*, 925.
[24] J. Zheng, H. Zhang, S. Dong, Y. Liu, C. T. Nai, H. S. Shin, H. Y. Jeong, B. Liu, K. P. Loh, *Nat. Commun.* **2013**, *5*, 2995.
[25] G. Eda, H. Yamaguchi, D. Voiry, T. Fujita, M. Chen, M. Chhowalla, *Nano Lett.* **2011**, *11*, 5111.
[26] J. Li, F. Ye, S. Vaziri, M. Muhammed, M. C. Lemme, M. Östling, *Carbon* **2012**, *50*, 3113.
[27] Y. T. Liang, M. C. Hersam, *J. Am. Chem. Soc.* **2010**, *132*, 17661.
[28] J. Li, M. Östling, *Crystals* **2013**, *3*, 163.
[29] R. D. Deegan, O. Bakajin, T. F. Dupont, G. Huber, S. R. Nagel, T. A. Witten, *Nature* **1997**, *389*, 827.
[30] C. Lee, H. Yan, L. E. Brus, T. F. Heinz, J. Hone, S. Ryu, *ACS Nano* **2010**, *4*, 2695.
[31] K. Levon, A. Margolina, A. Z. Patashinsky, *Macromolecules* **1993**, *26*, 4061.
[32] J. Li, B. Ray, M. A. Alam, M. Östling, *Phys. Rev. E* **2012**, *85*, 021109.
[33] A. Splendiani, L. Sun, Y. Zhang, T. Li, J. Kim, C.-Y. Chim, G. Galli, F. Wang, *Nano Lett.* **2010**, *10*, 1271.
[34] K. Zhou, Y. Zhu, X. Yang, J. Zhou, C. Li, *ChemPhysChem* **2012**, *13*, 699.
[35] W. Kim, A. Javey, O. Vermesh, Q. Wang, Y. Li, H. Dai, *Nano Lett.* **2003**, *3*, 193.
[36] D. J. Late, B. Liu, H. S. S. R. Matte, V. P. Dravid, C. N. R. Rao, *ACS Nano* **2012**, *6*, 5635.
[37] K. Lee, H.-Y. Kim, M. Lotya, J. N. Coleman, G.-T. Kim, G. S. Duesberg, *Adv. Mater.* **2011**, *23*, 4178.
[38] Z. Zeng, Z. Yin, X. Huang, H. Li, Q. He, G. Lu, F. Boey, H. Zhang, *Angew. Chem. Int. Ed.* **2011**, *50*, 11093.
[39] Q. He, Z. Zeng, Z. Yin, H. Li, S. Wu, X. Huang, H. Zhang, *Small* **2012**, *8*, 2994.
[40] Z. Yin, H. Li, H. Li, L. Jiang, Y. Shi, Y. Sun, G. Lu, Q. Zhang, X. Chen, H. Zhang, *ACS Nano* **2012**, *6*, 74.
[41] M. Freitag, J. C. Tsang, A. Bol, D. Yuan, J. Liu, P. Avouris, *Nano Lett.* **2007**, *7*, 2037.
[42] F. Xia, T. Mueller, Y.-M. Lin, A. Valdes-Garcia, P. Avouris, *Nat. Nanotechnol.* **2009**, *4*, 839.
[43] M. C. Lemme, F. H. L. Koppens, A. L. Falk, M. S. Rudner, H. Park, L. S. Levitov, C. M. Marcus, *Nano Lett.* **2011**, *11*, 4134.
[44] F. Xia, T. Mueller, R. Golizadeh-Mojarad, M. Freitag, Y.-M. Lin, J. Tsang, V. Perebeinos, P. Avouris, *Nano Lett.* **2009**, *9*, 1039.